The Cryosphere Discuss., 6, 759–792, 2012
www.the-cryosphere-discuss.net/6/759/2012/
doi:10.5194/tcd-6-759-2012


The Cryosphere Discussions



# Thin-layer effects in glaciological seismic amplitude-versus-angle (AVA) analysis: implications for characterising a subglacial till unit, Russell Glacier, West Greenland

**A. D. Booth[1], R. A. Clark[2], B. Kulessa[1], T. Murray[1], and A. Hubbard[3]**

[1]Glaciology Group, Department of Geography, College of Science, Swansea University, Singleton Park, Swansea, SA2 8PP, UK
[2]Institute of Geophysics and Tectonics, School of Earth and Environment, University of Leeds, Woodhouse Lane, Leeds, LS2 9JT, UK
[3]Institute of Geography and Earth Sciences, Aberystwyth University, Llandinam Building, Penglais Campus, Aberystwyth, SY23 3DB, UK

Received: 17 January 2012 – Accepted: 10 February 2012 – Published: 20 February 2012

Correspondence to: A. D. Booth (a.d.booth@swansea.ac.uk)

Published by Copernicus Publications on behalf of the European Geosciences Union.



## Abstract

Seismic amplitude-versus-angle (AVA) methods are a powerful means of interpreting the physical properties of subglacial material, although interpreting an AVA response is complicated in the case of a thinly-layered substrate. A layer thinner than one-quarter of the seismic wavelength is considered seismically "thin", and reflections from its bounding interfaces are perceived as a single event. Since a lodged (non-deforming) subglacial till can capped by a thin (metre-scale) cap of dilatant (deforming) till, serious misinterpretations can result if thin layer considerations are not honoured. AVA responses for layered subglacial tills are simulated: we model dilatant layers of thickness 0.1–3.0 m (up to a quarter-wavelength of our synthetic seismic pulse) overlying a lodged half-space, assigning typical acoustic impedance and Poisson's ratios to each. If thin layer effects are neglected, the AVA response to ultra-thin (<1.0 m) dilatant layers yields incompatible physical properties (acoustic impedance and Poisson's ratio indicating, respectively, a low- and high-porosity unit). We show an interpretative strategy that identifies thin layer effects and accurately quantifies the modelled acoustic impedance of lodged till from the composite AVA response. We apply this method to example seismic AVA data from the Russell Glacier outlet of the West Greenland Ice Sheet, in which characteristics of thin layer responses are evident. We interpret a stratified subglacial deposit, with upper and lower layers of high-porosity (<1.0 m thick, Poisson's ratio $>0.492 \pm 0.015$) and low-porosity (acoustic impedance of 4.20–$4.39 \times 10^6$ kg m$^{-2}$ s$^{-1}$) material, respectively assumed to represent dilatant and lodged tills. Thin layer considerations are strongly advised wherever seismic AVA analyses are used to quantify subglacial material properties.

## 1 Introduction

Characterising the physical properties of subglacial material is a key research goal for improving the representation of basal dynamics in predictive ice-flow models

(e.g. Pattyn, 1996; Truffer et al., 2001; Pimentel et al., 2011; Sergienko and Hulbe, 2011). Seismic reflection methods provide a powerful means of imaging the bed of glaciers and ice masses, and are increasingly used for quantifying substrate material properties (e.g. Smith, 1997; Nolan and Echelmeyer, 1999; Anandakrishan, 2003; Peters et al., 2008). Seismic amplitude-versus-angle (AVA) analysis is particularly useful, having the potential to measure at least two mechanical properties of a subglacial material, specifically its acoustic impedance and Poisson's ratio (Aki and Richards, 2002; Gretener, 2003) (note: AVA exploits the same seismic characteristics and principles to amplitude-versus-offset, AVO, but expresses the variation of reflectivity with actual incidence angle rather than its offset proxy). AVA has had notable use in glaciology for identifying subglacial lakes (Peters et al., 2008), thick sequences of dilatant (deforming) till (Anandakrishnan, 2003) and transient changes in subglacial hydrology (Nolan and Echelmeyer, 1999; Kulessa et al., 2008).

Seismic AVA analysis has several key assumptions, a number of which can be violated when analysing the response over a subglacial till unit. A till deposit can be highly complex, with abrupt variations (both vertical and lateral) in physical properties (Evans et al., 2006) that, critically for seismic interpretation, can be present on a smaller spatial scale than the wavelength of the seismic wavelet (~10 m in glaciology, depending on source characteristics and ice thickness; Smith, 1997). Such small-scale variations greatly complicate the interpretation of an AVA response (Swan, 1991; Bakke and Ursin, 1998; Nolan and Echelmeyer, 1999) and, in this paper, we consider how reliably a "thinly-layered" till deposit can be characterised in seismic data.

Although AVA practitioners within glaciology may be aware of the potential for such problems (e.g. Richards, 1988; Nolan and Echelmeyer, 1999), there have been few reported investigations of how "thin layer" AVA responses manifest themselves or how they can subsequently be interpreted. Here, we review AVA theory and consider the definition of "thin", from a seismic perspective. We then use synthetic seismic data, simulating an acquisition over dilatant (deforming) and lodged (non-deforming) subglacial till layers (e.g. Evans et al., 2006; Peters et al., 2007), to show how the AVA



response is complicated by such thin stratifications. This analysis leads to the proposal of a strategy for interpreting subglacial properties from thin layer AVA responses, which we then apply in (a) analysis of new seismic data from an outlet glacier of the West Greenland Ice Sheet and (b) an alternative suggestion for a till structure beneath an Antarctic ice stream, compared to that proposed by Peters et al. (2007). Thin layer considerations are vital for accurately interpreting the physical properties of subglacial till deposits, and we highlight the serious misinterpretations that may result if they are neglected.

## 2 Reflection coefficients and amplitude-versus-angle responses

A seismic wavelet undergoes a partial reflection when it encounters an interface between contrasting acoustic properties. The fraction of energy reflected, termed the "*reflection coefficient*", $R$, is influenced both by the magnitude of that contrast (specifically in terms of the velocities of P-(primary) and S-(shear) waves, density and, to a lesser extent, seismic quality factor, $Q$), and the incidence angle at which the wavelet arrives. For a wavelet propagating at normal incidence (i.e. $\theta = 0$) from the $i$th to the $j$th layer, the P-wave reflection coefficient is a simple function of the acoustic impedance within each layer:

$$R(0) = \frac{Z_j - Z_i}{Z_j + Z_i} \tag{1}$$

where $Z$ denotes acoustic impedance, the product of density and P-wave velocity, $v_P$ (note: transitions between highly contrasting (e.g. an order-of-magnitude or more) quality factors may also contribute to the observable reflectivity of an interface (Odebeatu et al., 2006; Quintal et al., 2009; Morozov, 2011)). However, in the general case of non-normal incidence (i.e. $\theta > 0$), a fraction of the incident P-wave is also converted to

S-wave energy, hence reflectivity is also influenced by Poisson's ratio, $\sigma$:

$$\sigma = \frac{\left(v_p/v_S\right)^2 - 2}{2\left(\left(v_p/v_S\right)^2 - 1\right)}, \quad (2)$$

where $v_S$ is S-wave velocity (note: as S-wave velocity approaches zero (i.e. its velocity through water), Poisson's ratio reaches its theoretical maximum of 0.5). The general expression for $R(q)$ is the "*Knott-Zoeppritz equation*", a complicated, non-linear function of angle and acoustic properties (Aki and Richards, 2002) and the variation of reflected amplitude with angle is termed the "*AVA response*".

Figure 1 shows AVA responses modelled for glacier beds underlain by material of varying (a) acoustic impedance and (b) Poisson's ratio (see Table 1); in all cases, the acoustic impedance and Poisson's ratio of the overlying ice are fixed at $3.50 \times 10^6\,\mathrm{kg\,m^{-2}\,s^{-1}}$ (Peters et al., 2008) and 0.33 (Anandakrishnan, 2003) respectively. Note, for reference, AVA curves for ice-rock and ice-water interfaces are also included as these represent end-member contrasts in typical glaciological settings.

Where acoustic impedance of the substrate exceeds that of the overlying ice, the zero-incidence reflection coefficient is positive (Fig. 1a, models *i*-*iv*), switching to negative (i.e. a polarity reversal) between 40–55° incidence; these "zero-crossings" can be highly diagnostic of material properties (Anandakrishnan, 2003). In Fig. 1b, since $Z$ is fixed, all models express equal $R(0)$ but express different AVA gradients (e.g. strongly negative in model *i* and strongly positive in model *v*, at least up to $\theta = 55°$). As shown in these models, strongly positive AVA gradients indicate high Poisson's ratios in the subsurface, as associated with water-saturated sediment (S-waves propagate more slowly in wet materials, leading to increases of $v$ in Eq. 2).

The characteristics of numerous AVA responses can be summarised on an "*AVA cross-plot*" (Simm et al., 2000) (Fig. 1c for previous model curves). Shuey (1988) linearises the Knott-Zoeppritz equations, simplifying the angular variation in reflectivity



as:

$$R(\theta) = A + B\sin^2(\theta), \quad (3)$$

where $A$ and $B$ are functions of velocity and density contrasts. $A$ and $B$ are estimated by linear regression on the AVA curve plotted against $\sin^2(\theta)$. This linearisation is most appropriate in cases of negligible refraction, i.e. for $\theta$ up to ~30°, and for small velocity contrasts. Our models, and typical contrasts across the bed of a glacier, violate this latter condition, hence $A$ and $B$ cannot be used to quantify velocity and/or densities. However, the AVA cross-plot still serves as an efficient means of highlighting qualitative characteristic trends between families of AVA curves. Best-fit Shuey terms are therefore derived and cross-plotted (Fig. 1c) for each curve in Fig. 1a and b (cross and circle symbols, respectively). Changes to acoustic impedance have the greatest effect on $A$ (which approximates R(0)), whereas changes to Possion's ratio only modify $B$. We return to the AVA cross-plot in later analysis, when comparing synthetic AVA responses.

## 3 Thin layers in glaciological AVA analysis

The Knott-Zoeppritz equations are strictly defined for the interface between two otherwise infinite, homogeneous, isotropic, half-spaces, and the presence of "thin layers" between these half-spaces violates this assumption (Bakke and Ursin, 1998; Aki and Richards, 2002; Nolan and Echelmeyer, 1999). In seismic terms, a layer is considered "thin" if it is thinner than one-quarter wavelength of the seismic wavelet (Widess, 1973). At this threshold, termed the "tuning thickness" (Widess, 1973), reflections from the upper and lower interfaces of the layer superpose and a single interface is perceived. For thinner layers, around one-eighth of the wavelength, the composite response approximates the derivative of the original signal (Bakke and Ursin, 1998), and further thinning also reduces its amplitude (Bakke and Ursin, 1998). For these "ultra-thin" layers, the composite response may also be influenced by intrabed multiples and

mode conversions (i.e. respectively, wavelets that reverberate within the thin layer, and those that are converted between P- and S-wave modes). Thin bed effects introduce significant potential for misinterpretation, and Swan (1991) cautions that their impact can be stronger than the intrinsic lithological AVA effect.

Would thin-layer problems be commonplace in glaciological seismic investigations? With a typical seismic wavelength of ∼10 m (Smith et al., 1997; Anandakrishnan, 2003; Horgan et al., 2008), vertical stratifications spaced more closely than a small number of metres would be considered seismically "thin". Although glaciers themselves are clearly good approximations to half-spaces, subglacial tills frequently contain metre- (or sub-metre-) scale contrasts (Smith, 1997), such as the transitional boundaries between dilatant (deforming) and lodged (non-deforming) (e.g. Clarke et al., 1984; Echelmeyer and Wang, 1987; Iverson et al., 1988, 1994; Truffer et al., 2000; Boulton et al., 2001; Porter and Murray, 2001; Evans et al., 2006; Iverson, 2011; Reinardy et al., 2011). It would therefore be prudent to consider how such fine-scale layering affects a seismic AVA response whenever surveys are conducted over till substrates.

Numerous strategies, developed principally in the hydrocarbon sector but also in glaciology, are available for interpreting thin layer AVA responses, although simplifications and/or assumptions that these make may be inappropriate in glaciological settings. Lin and Phair (1993) quantify the properties of a thin layer located in an otherwise homogeneous half-space, assuming that its upper and lower interfaces therefore have equal-magnitude reflection coefficients. This is clearly unsuitable in glaciology, where a thin layer of dilatant till is bounded by ice and lodged till, respectively. Richards (1988) and Nolan and Echelmeyer (1999) derive generalised analytic expressions for thin-layer AVA responses by summing infinite series of intrabed multiples, but this approach effectively imposes an infinite quality factor (i.e. neglects wavelet attenuation). More realistically, a finite quality factor would more-rapidly attenuate intrabed multiples, and distort the interference pattern given the progressive extension of wavelet period. Here, we decompose the composite AVA response to a thin layer geometry using three approaches:



1. travel-time analysis of the reflected wavelets that contribute to the composite response,
2. assessment of the effective reflectivity of those reflections using the Knott-Zoeppritz equation, and
3. full-waveform forward modelling of thin layer seismic responses.

### 3.1 Ray-tracing of reflected travel-times

We ray-traced travel-times for an isotropic, homogeneous glacier, overlying a horizontal, isotropic, layer of dilatant till and a lodged till half-space (model parameters listed in Table 2); the ice is 1 km thick, although the AVA response is independent of ice thickness provided that the relative range of offsets is maintained. Material properties of ice, dilatant and lodged till were taken from Peters et al. (2008); the acoustic impedance of the dilatant till is within the plausible range specified by Vaughan et al. (2003), and its Poisson's ratio is 0.494, typical for water-saturated sediment (Gercek, 2007). In Sect. 3.3, our synthetic source wavelet has a dominant frequency of 150 Hz (matching the pulse observed in later analysis of field data) and a nominal wavelength, $\lambda$, of 12 m in the dilatant till ($v_P = 1800\,\mathrm{ms}^{-1}$). We therefore extend the thickness of the dilatant till layer, $h_d$, from 0.1 m to 3.0 m, i.e. from an ultra-thin layer ($h_d << \lambda/8$) to the theoretical limit of resolution of the dominant wavelength of the synthetic seismic wavelet.

Travel-times for nine reflected raypaths (Fig. 2) were calculated for sources and receivers offset in a common-midpoint (CMP) configuration from 0 to 5000 m (0–68° basal incidence, for the 1 km ice thickness). The nomenclature of each raypath describes the mode (i.e. P- or S-wave) of the wavelet as it crosses an interface; we only consider raypaths that arrive at the surface as P-waves, since S-waves travel more slowly through ice ($v_S \approx 0.5\,v_P$) hence do not interfere with the base-ice reflection, ***PP***. Critical refractions are not considered since, at each interface and for each wavelet mode, incidence angles are sub-critical.

Example travel-times for $h_d = 3.0$ m are shown in Fig. 3a, plotted for clarity as a lag behind the arrival time of ***PP***. The lag is almost-constant for each raypath, given that they are strongly refracted towards vertical across the ice-till interface (for ***PP*** impinging at 68°, ***PPPP*** and ***PSSP*** are refracted to 27.8° and 3.0°, respectively). At this theoretical limit of resolution, the two-way travel-time of a P-wave through the dilatant till layer is 3.4 ms (grey shading), hence only raypaths that lag ***PP*** by less than this can interfere and therefore contribute to the composite AVA response. Here, ***PPPP*** arrives just beyond this lag, supporting the theoretical assumption that $h_d = 3.0$ m is indeed the limit of resolution in our study. Equivalent models for thinner layers are shown, along with relevant synthetic data, in Fig. 4.

### 3.2 Effective reflectivity

Deriving the individual AVA responses of these reflections allows their specific contributions to be identified within the composite AVA response. We use the Knott-Zoeppritz equations to obtain the *effective* reflectivity (i.e. honouring all of the reflection and transmission coefficients accrued by the time the wavelet emerges from the till unit) of the nine reflections in Fig. 2 (Fig. 3b), and plot this against the ***PP*** incidence angle (as would be performed if only a single reflection was resolved).

The base ice reflection (***PP***) shows AVA characteristics expected from a transition from low-to-high $\sigma$ and high-to-low $Z$, specifically negative $R(0)$ (= −0.011), positive AVA gradient (here, for $\theta < 50°$) and a polarity reversal (here, at $\theta \approx 10°$). The P-wave reflection from the internal till interface (***PPPP***) has the opposite character (positive $R(0) = +0.066$ and negative AVA gradient), although P-wave reflectivity within the dilatant till is low and its intrabed multiples are negligible. However, the equivalent reflectivity for S-waves is much higher; ***PSSP*** is very strong at 60° incidence (4-times stronger than the maximum magnitude of ***PP***) and its multiple wavetrain remains significant even after two reverberations. However, the successively reversed polarity of S-wave intrabed multiples causes them to interfere destructively, thereby limiting their potential for interference.



Together, travel-time and reflectivity models suggest that the strongest contributions to the composite AVA response will be ***PP*** and ***PPPP***, with weaker contributions from ***PSPP, PSSP***, and intrabed multiples of the latter in the ultra-thin layer cases.

### 3.3 Forward modelling of seismic data

Although they provide valuable insight into the overall character of a composite AVA response, the previous modelling approaches assume infinite quality factor, and impose no attenuation on the propagating wavelet. We therefore forward-modelled seismic responses using the software "*SKB2*" (Laboratoire de Géophysique Interne et Tectonophysique, University of Grenoble; Kennet and Kerry, 1979; Bouchon, 1981; Kennet, 1983; Mallick and Frazer, 1987), which delivers the three-component (i.e. vertical, radial and transverse) seismic response to a one-dimensional reflectivity model (homogenous, isotropic, horizontal layering) for any prescribed range of CMP offsets. Here, we consider only the vertical component of the seismic wavelet since geophones in our field data (Sect. 5) recorded only that component.

As in previous modelling, we assume a source pulse of 150 Hz frequency and CMP offsets from 0 to 5000 m, and the physical properties listed in Table 2. The P-wave quality factor ($Q_P$) is measured from seismic data (Sect. 5) and, in the absence of a reference value for the S-wave quality factor ($Q_S$), we assume $Q_S = Q_P$ (e.g. Abercrombie and Rice, 2005) (although, as stated, S-waves that propagate in ice are of secondary importance here). There appear to be no reported examples of either $Q_P$ or $Q_S$ for in situ subglacial till hence, for each thickness model, we produce three sets of seismic responses assuming different attenuation. First, we assume that the till is essentially non-attenuating, fixing $Q_P = Q_S = 10^4$ (termed "$Q_\infty$"). Thereafter, we impose two sets of quality factors (see Table 2) derived in the hydrocarbon industry for unconsolidated sea-floor mud (Best et al., 1994; Ayres and Theilen, 2001; Riedel and Theilen, 2001; Sain and Singh, 2011), simulating high-$Q$ ("$Q_H$") and low-$Q$ ('$Q_L$') regimes. This analogue is considered appropriate, particularly given that the pore-pressure regime in

sea-floor sediment is more likely to be representative of that beneath an ice sheet, than a measurement made on a surface till exposure.

Selected forward-modelled seismic responses are shown in Fig. 4 ($Q_\infty$, $Q_H$ and $Q_S$ models, respectively, in rows a, b and c), together with the appropriate ray-traced travel-time model (again, the grey shading indicates the 3.4 ms lag at the $\lambda/4$ resolution threshold). An amplitude scalar is derived and applied to each trace, assuming propagation in ice only, to correct for geometric spreading and attenuation losses (in which the attenuation rate of the dominant 150 Hz frequency is assumed). Displayed travel-times again correspond to the lag behind ***PP***, following the application of non-stretch normal-moveout (NMO) corrections (Perroud and Tygel, 2005), assuming $v_P = 3800\,\mathrm{ms}^{-1}$ (e.g. Peters et al. (2008), and measured from data in Sect. 5). A control response is included in each figure for comparison, corresponding to ice overlying a non-attenuating dilatant till half-space (i.e. $h_d = \infty$). For $Q_\infty$ and $Q_H$ models, these control responses express the reflectivity of ***PP*** (Fig. 3b), having a polarity reversal at 10° incidence and increasing wavelet amplitudes up to 50° incidence; the control response for $Q_L$ is somewhat distorted given the strong $Q$-contrast across the glacier bed interface, and the polarity reversal is shifted to ∼25° incidence.

$Q_\infty$ and $Q_H$ responses appear very similar. Only for the thickest layers of dilatant till ($h_d > 2.0$ m) can the characteristics of ***PP*** be resolved whereas, for thinner layers, no polarity reversal is apparent and stronger reflectivity is observed across the first 30° of incidence. $Q_L$ responses show characteristics of ***PP*** throughout since the strong subglacial attenuation suppresses the other reflections, and the polarity reversal is clear for all but the thinnest layer cases.

For $h_d = 0.1$ m, all reflections arrive within 3.4 ms of ***PP*** hence all contribute to the composite AVA response. However, where $h_d \geq 1.0$ m, any arrival that features an S-wave mode conversion is delayed from ***PP*** by more than 3.4 ms, hence the composite AVA response is dominated by P-wave reflectivity alone. Furthermore, since the reflectivity of P-wave intrabed multiples is negligible, the composite response is principally a hybrid of ***PP*** and ***PPPP*** until the thin-layer can be resolved.



### 3.4 Composite AVA curves

The composite AVA curves derived from all modelled data are shown in Fig. 5 (upper and lower rows showing $[h_d < \lambda/8]$ and $[\lambda/8 \leq h_d \leq \lambda/4]$, respectively; effective reflectivities of ***PP*** and ***PPPP*** are also shown, for reference). Amplitudes of synthetic wavelets are picked at the absolute maximum of the first identifiable half-cycle (grey triangles in Fig. 4; note that these are low since we impose the smallest likely acoustic impedance contrast, ($0.08\,\mathrm{kg\,m^{-2}\,s^{-1}}$), between the ice and dilatant till given the ranges in Peters et al., 2008). The composite $R(0)$ was obtained by comparing each zero-incidence amplitude to its equivalent in the control model, in which $R(0)$ is explicitly known (i.e. from substituting $Z$ for ice and dilatant till into Eq. 1). Since wavelet amplitude scales linearly with reflection coefficient, the ratio of amplitudes is equivalent to the ratio of reflection coefficients.

Again, there is a strong similarity between $Q_\infty$ and $Q_H$ AVA responses (5a and b). For $h_d < 1.0$ m, these show a positive AVA gradient for the first 40° incidence, and $R(0)$ close to that of ***PPPP***. Equivalent curves for $h_d \leq 2.5$ m show similar responses to ***PP***, consistent with the thin layer becoming resolved; however, the maximum observed reflectivity never reaches that of ***PP*** since we consider only the vertical component of the seismic wavelet (as incidence angle tends towards horizontal, an increasing proportion of P-wave particle motion is in the radial direction). More complex responses are observed as $h_d$ approaches and exceeds $\lambda/8$ (i.e. between 1.0 and 2.0 m), which feature an abrupt switch in AVA gradient at ∼10° incidence and an approximation to the reflectivity of ***PP*** thereafter. The position of the switch is clearly similar to that of polarity reversal in ***PP***, and the increased reflectivity observed at $\theta < 10°$ is attributed to interference between ***PP*** and ***PPPP***; an S-wave explanation is rejected because ***PSSP*** has low reflectivity at small incidence angles.

$Q_L$ responses (Fig. 5c) are markedly different; consistent with observations in Fig. 4c, each curve approximates the general form of ***PP*** albeit shifted towards more-negative reflectivity. Interference effects in these models differ strongly from the previous models, given the extreme attenuation in the till.

We now revisit the AVA cross-plot (Fig. 5d), showing how composite AVA reflectivity varies from model to model. Best-fit Shuey terms are derived for each model, for incidence angles from 0–30° (for comparison, examples from Fig. 1c and the effective reflectivity of ***PP*** and ***PPPP*** are also shown); error bars show the standard uncertainties in the linear regression. The difference between best-fit terms to $Q_L$ (green) models, and those to $Q_\infty$ (blue) and $Q_H$ (red), is again striking. $Q_L$ models progressively drift from ***PP*** with increasing $h_d$, although that drift is principally in the $A$-direction implying that AVA gradients are similar and the biggest change is in $R(0)$. For $Q_\infty$ and $Q_H$, where $h_d < \lambda/8$, best-fit terms plot between those of ***PP*** and ***PPPP***; as $h_d$ approaches and exceeds $\lambda/8$, these drift to more-positive $A$ and more-negative $B$ (note that the uncertainty in the fit also grows, given the gradient switch within the first 30° of incidence). Finally, as $h_d$ approaches $\lambda/4$, the thin layer starts to be resolved and $A$ and $B$ move closer to those of ***PP***. We next consider these observations in terms of their implications for glaciological interpretation.

## 4 Glaciological interpretation of thin layer responses

Seismic AVA interpretation of a till unit is clearly sensitive to changes in its overall composition, but also to the thickness of overlying dilatant layers and the attenuation regime. The key issue for interpretation is that the composite response to a stratified till deposit can resemble a geophysically plausible response to a single interface, and hence may be misdiagnosed as such.

Table 3 shows the scale of such a misinterpretation for the acoustic impedances and Poisson's ratios, as modelled with in the previous sections. For acoustic impedance, Eq. (1) is rearranged for $Z_j$ and, by substituting observed $R(0)$ values and the known acoustic impedance for ice, we calculate the apparent acoustic impedance, $Z_{app}$, of a single substrate layer. $Z_{app}$ is then compared to model acoustic impedances of both the dilatant and lodged till layers, to assess which are best-represented. For Poisson's ratio, a grid-search is performed by substituting trial parameters into the Knott-Zoeppritz



equations, to establish the best-fit curve to each composite AVA response. The corresponding seismic velocities are then used to define an apparent Poisson's ratio, $\sigma_{app}$. Clearly, the apparent properties are not always suggestive of either dilatant or lodged till, and the following discussion considers the cases where they can be recovered.

### 4.1 $Q_\infty$ and $Q_H$ models

For the less attenuating models, for the thickest $h_d$ (≤2.5 m) cases, AVA responses accurately express both $Z_{app}$ and $\sigma_{app}$ of the dilatant till since ***PP*** can be resolved from ***PPPP***. The intermediate layer thicknesses ($h_d$ between 1.0 and 2.5 m) yield better approximations of the Poisson's ratio of dilatant till, but acoustic impedance is not clearly diagnostic of either till. However, the AVA responses associated with these geometries are obviously more complex than those from single interfaces and would therefore not be interpreted as such.

The interpretative risk is most significant for the ultra-thin $h_d$ geometries (<1.0 m), since their plausible AVA curves yield $Z_{app}$ similar to that of the underlying lodged till (within ∼ ±2 %) but $\sigma_{app}$ more representative of the dilatant till (within −10 %). If we used single-interface AVA analysis (i.e. ignoring thin layer effects), we would conclude that the glacier was underlain by a lodged till with a high Poisson's ratio. However, in a glaciological context, these are mutually inconsistent conclusions compared to published examples of till substrates (e.g. Smith et al., 1997; Vaughan et al., 2003). Invoking a thin layer approach can resolve this incompatibility: we propose the following strategy for characterising the substrate in these cases.

In Fig. 5c, the best-fit Shuey terms for the ultra-thin geometries plotted between those of ***PP*** and ***PPPP***, suggesting the composite $A$ and $B$ values somehow average those of the model. Measuring zero-incidence reflectivities from Fig. 5a and b shows that the observed values approximate the sum of the effective zero-incidence reflectivity at the two model interfaces (−0.011 and +0.066 at the ice-till and internal-till interfaces, respectively, with a sum of +0.055). This approximation is very good for $Q_\infty$ models where, for $h_d$ of 0.1 m, 0.3 m and 0.5 m, the apparent zero-incidence

reflectivity, $R_{app}(0)$ is +0.055, +0.054 and +0.056 respectively (Fig. 5a). The approximation is somewhat worse for $Q_H$ models, given the increased attenuation, and equivalent $R_{app}(0)$ values are +0.045, +0.043 and +0.046 respectively (Fig. 5b). However, with measured (or reference) acoustic impedances for ice and dilatant till ($Z_{dilatant}$, here = $3.90 \times 10^6$ kg m$^{-2}$ s$^{-1}$), $R_{app}(0)$ can be decomposed into contributions from the ice-till and internal-till interfaces:

$$R_{app}(0) = R_1(0) + [1 - R_1(0)]^2 R_2(0) \quad (4)$$

$$= R_1(0) + [1 - R_1(0)]^2 \frac{Z_{lodged} - Z_{dilatant}}{Z_{lodged} - Z_{dilatant}}, \quad (5)$$

where $R_1(0)$ and $R_2(0)$ are, respectively, the effective zero-incidence reflectivities of the ice-till (−0.011) and internal-till (+0.066) interfaces, and $Z_{lodged}$ is the acoustic impedance of the underlying lodged till. Rearranging for $Z_{lodged}$ therefore gives:

$$Z_{lodged} = \frac{Z_{dilatant}[(R_{app}(0) - R_1(0)) + [1 - R_1(0)]^2]}{[1 - R_1(0)]^2 - (R_{app}(0) - R_1(0))}. \quad (6)$$

When substituted into Eq. (5), the apparent reflectivities from the ultra-thin $Q_\infty$ models deliver $Z_{lodged}$ with negligible error; the equivalent values from the $Q_H$ models, with $h_d$ of 0.1 m, 0.3 m and 0.5 m, yield $Z_{lodged}$ of $3.81 \times 10^6$ kg m$^{-2}$ s$^{-1}$, $3.80 \times 10^6$ kg m$^{-2}$ s$^{-1}$ and $3.82 \times 10^6$ kg m$^{-2}$ s$^{-1}$ (errors of −2.31 %, −2.56 % and −2.05 %) respectively. The acoustic impedance of the lodged till is therefore well-characterised despite the higher attenuation losses.

The Poisson's ratios for the two layers are less easily decomposed, although it is clear that composite response suggests $\sigma_{app}$ much-closer to that of the dilatant till. At this stage of analysis, we simply recommend stipulating that the Poisson's ratio implied by the composite response is the lower limit of that of the dilatant till layer.



### 4.2 $Q_L$ models

Responses to $Q_L$ models clearly represent the Poisson's ratio of the dilatant till (within ∼6 %), although the apparent acoustic impedance corresponds neither to dilatant nor lodged till; furthermore, $Z_{app}$ is biased to increasingly small values even as $h_d$ approaches its resolvable threshold, suggesting an influence of $Q$-based reflectivity (Odebeatu et al., 2006; Morozov, 2011). However, improving the understanding of $Q$ contributions requires better constraint of the attenuation characteristics of subglacial till, rather than the sea-floor analogue we impose at this stage. Nonetheless, it appears that there is never the risk that dilatant till could be misdiagnosed as lodged till in the case of extreme attenuation, although the physical properties assigned thereafter may be inaccurate. The interpretative problem is instead that the thickness of the dilatant till layer could be over-estimated, with dilatant characteristics assigned through the whole depth of the till deposit.

## 5 Application to real data

We now consider thin layer effects in the AVA analysis of actual seismic data, acquired on the Russell Glacier outlet of the West Greenland ice sheet (∼70 km inland of its western margin) during summer 2010. At the position of the AVA analysis, the ice is 1.08 ± 0.01 km ($v_P$ = 3800 ± 40 ms$^{-1}$) thick and the bed reflection is planar over ∼750 m with an in-line dip less than 3°.

Figure 6a shows a representative shot gather (one of 46) from this acquisition (note: a shot gather is presented since our CMP gathers comprised 6 traces only; nonetheless, each reflection point is within the range of the bed used in the following AVA analysis). Sources were 250 g Pentex charges, installed along the line, at ∼3 m depth, at 80 m intervals, and data were recorded with a Geometrics *GEODE* system at 48 concrete-mounted, 100 Hz, vertical-component geophones installed at 10 m intervals. As in Fig. 4, trace amplitudes are scaled for geometric spreading and attenuation

losses ($Q_P = 436 \pm 140$, as measured using spectral ratios between primary and multiple arrivals; Dasgupta and Clark, 1998; Gusmeroli et al., 2010); further data processing involves the removal of a 25 ms detonator delay, and bandpass filtering to enhance signals within the useful wavelet bandwidth (centred on 150 Hz). For the measured ice thickness and $v_P$ (assumed constant), the 400 m offset range of this record corresponds to an incidence range of 6–17° at the glacier bed. For these angles, and elsewhere in the record (up to a maximum incidence angle of ~23°), the basal reflection shows no polarity reversal, immediately excluding a dilatant till substrate in a conventional (i.e. neglecting thin layers) AVA analysis.

An AVA response is derived across a 300 m wide section of the glacier bed (Fig. 6b); although this produces a spatially-averaged basal reflectivity, our wavelets have a Fresnel zone (Lindsey, 1989) of 165 m, hence the range of this averaging does not greatly exceed the intrinsic resolution in our seismic data. The signal-to-noise ratio of the response is enhanced further by averaging bed reflectivity in 1° incidence angle bins (Peters et al., 2008), with error bars spanning the interquartile range of the reflectivity and incidence angle within each bin (Booth et al., 2011; key sources of error are coupling variability and the uncertainty in $v_P$, ice thickness and $Q_P$). The measurement of zero-incidence reflectivity followed the method of King et al. (2003), in which the amplitude of primary and multiple reflections are compared for a 0–10° incidence range.

The AVA response shows both positive $R(0)$ and gradient; accordingly, both $A$ and $B$ in the Shuey best-fit linearisation are also positive (cross-plotted in Fig. 10c; previous examples and models also included). The best-fit Knott Zoeppritz curve through the AVA response (established from a grid-search with ice properties fixed at $v_P$, $v_S$ and density of $3800 \pm 40\,\mathrm{ms}^{-1}$, $1898 \pm 40\,\mathrm{ms}^{-1}$ and $920\,\mathrm{kg\,m}^{-3}$, respectively) suggests the substrate has acoustic impedance of $[4.37 \pm 0.05] \times 10^6\,\mathrm{kg\,m}^{-2}\,\mathrm{s}^{-1}$ and Poisson's ratio of $0.492 \pm 0.015$. The acoustic impedance is therefore indicative of a low-porosity, unlithified till (Vaughan et al., 2003), but this is contradicted by the Poisson's ratio which implies a dilatant, water-rich, till (Gercek, 2007; Peters et al., 2008). These



observations suggest that the AVA response is a thin layer composite, and hence that the substrate is a layered till unit. We therefore reinterpret these data as such, with reference to previous models.

There is a striking similarity between the real-data AVA response and those of the ultra-thin geometries in the $Q_\infty$ and $Q_H$ models (cf. Fig. 5a, b with 6b ,c). Exploiting this similarity, the dilatant till is assumed to have a maximum thickness of 1.0 m and attenuation to be less than that in the $Q_L$ simulations; we then interpret the AVA response using Eq. (5), to predict the likely acoustic impedance of the underlying layer. Figure 6b shows $R_{app}(0) = +0.1163$. We use reference values of the acoustic impedance of dilatant till as provided by Vaughan et al. (2003), specifically $Z_{dilatant} = 3.0\text{–}3.4 \times 10^6\,\mathrm{kg\,m}^{-2}\,\mathrm{s}^{-1}$, and, with measured ice properties, obtain the range of $R_1(0)$ from −0.076 to −0.014. On substituting these quantities into Eq. (5), we predict that the acoustic impedance of the underlying layer is between $4.20\text{–}4.39 \times 10^6\,\mathrm{kg\,m}^{-2}\,\mathrm{s}^{-1}$, suggestive of a low-porosity, lodged till unit (Vaughan et al. 2003). The minimum Poisson's ratio of the dilatant till is $0.492 \pm 0.015$, which approaches the theoretical limit of $\sigma$ and therefore indicates a highly water-rich layer.

## 6 Discussion and implications

Our observations facilitate a greater degree of complexity in the interpretation of glaciological AVA responses. Although our interpretation is based on qualitative similarities to model outputs, a meaningful numerical inversion would require measurement or assumption of additional properties, particularly $Q_P$ and $Q_S$ for subglacial till (and glacier ice in the latter case). We acknowledge that we assume homogenous and isotropic layer properties throughout, having measured both $v_P$ and $Q_P$ from depth-averaged observations (in the former case, by pre-stack migration velocity analysis (Sheriff and Geldart, 1999; Bradford et al., 2009)). Research has shown detectable englacial velocity and attenuation contrasts that correspond to changes in ice temperature (Kohnen, 1974; Peters and Anandakrishnan, 2010) and/or crystal orientation (Horgan et al.,

2008), the latter of which may give rise to anisotropy thereby complicating AVA interpretation (e.g. Tsvankin, 2001). However, we consider that initial recognition of thin layer issues provides a significant improvement over a conventional interpretation approach. Alternative quantitative approaches to deriving the actual thickness of the thin layer include spectral and/or cepstral relationships (e.g. Hall, 2006; Rubino and Velis, 2009) but these typically require higher signal-to-noise ratio than is present in our data.

While seismic methods are clearly able to quantify the physical properties of in situ subglacial material, care is required to ensure that subtle variations in those properties are not misinterpreted and the potential for thin layer effects should be recognised. This is particularly relevant where the interpretation is supplied to predictive models of glacier flow, given the sensitive relationship between the substrate of a glacier and its flow regime (Pattyn, 1996; Truffer et al., 2001; Pimentel et al., 2011; Sergienko and Hulbe, 2011). For a glacier underlain by (and potentially frozen to) bedrock, thin layer issues are less significant since the substrate is unlikely to be strongly stratified. Likewise, they are irrelevant in AVA studies of subglacial lakes (Peters et al., 2008), provided that the free-water thickness exceeds the quarter-wavelength limit of resolution.

Thin layer considerations are strongly recommended, however, where AVA methods are used to characterise subglacial till, and particularly when used to identify local, lateral, changes in till properties (e.g. Peters et al., 2007; Smith et al., 2007). For example, Peters et al. (2007) use AVA methods to interpret the stiffness of a 5–20 m thick till unit beneath Bindschadler Ice Stream (BIS), West Antarctica. The theoretical limit of resolution of their wavelet is 5 m, hence reflections from the interfaces of the till unit can be resolved throughout, and no thin layer considerations are made. Basal AVA responses indicate discrete, kilometre-scale, lateral variations (150 $\mathrm{ms}^{-1}$, 800 $\mathrm{ms}^{-1}$ and 150 $\mathrm{kg\,m}^{-3}$ in $v_P$, $v_S$ and density, respectively) in till properties, which are interpreted as "cycles" (transitions) between wet and stiff till regimes. Thin layer considerations offer an alternate interpretation, that BIS is underlain by a stratified till unit, composed principally of stiff till but with a wet till "cap", and the seismic variability is explained by lateral variations in the thickness (from 0 to 5 m) of the latter. These interpretations represent



end-member arguments: neglecting thin layers accommodates all of the seismic variability in a lateral change in till composition, whereas invoking thin layers attributes that variability to a lateral change in stratification. Whilst an explanation in terms of later variation only is possible, we suggest that our modified interpretation is more consistent with recent observations of stratifications in subglacial tills, in which deformation is restricted to an upper, dilatant layer of metre-scale thickness (Piotrowski et al., 2004; Evans et al., 2006; Iverson et al., 2011; Reinardy et al., 2011).

## 7 Conclusions

Seismic AVA analysis is a powerful method for quantifying the physical properties of subglacial material, although serious misinterpretations can result when applied over layered substrates. Here, we have shown how thin layer effects manifest themselves in glaciological AVA responses, and how they can then be interpreted in terms of the thickness, acoustic impedance and Poisson's ratio of the subglacial material. The recognition of thin layer AVA issues is a major step forward in improving the potential to image and characterise the subglacial environment, a key aspect given the importance of subglacial processes in predictive ice flow models. We would therefore recommend that thin layer analyses form a routine part of AVA investigations, particularly where stratified subglacial deposits are anticipated.

*Acknowledgements.* ADB is funded by a Leverhulme Trust Research Leadership project, F/00391/J. Field campaign supported by: Greenland Analogue Project: Sub-Project A, funded by SKB, Posiva and NWMO; Natural Environment Research Council grants NE/G007195/1 and NE/H0126889/1. Landmark Strategic University Alliance grants *ProMAX*™ access to the University of Leeds, under agreement 2004-COM-024982. Data acquisition would have been impossible without the efforts of Alessio Gusmeroli, Christine Dow, Sam Doyle and Glenn Jones. Constructive discussions with Benedict Reinardy during manuscript preparation were greatly appreciated.

## References


Abercrombie, R. E. and Rice, J. R.: Can observations of earthquake scaling constrain slip weakening?, Geophys. J. Int., 162, 406–424, doi:10.1111/j.1365-246X.2005.02579.x, 2005.

Aki, K. and Richards, P. G.: Quantitative Seismology, University Science Books, 2nd Edition, 2002.

Anandakrishnan, S.: Dilatant till layer near the onset of steaming flow of Ice Stream C, West Antarctica, determined by AVO (amplitude vs offset) analysis, Ann. Glaciol., 36, 283–286, 2003.

Ayres, A. and Theilen, F.: Preliminary laboratory investigations into the attenuation of compressional and shear waves on near-surface marine sediments, Geophys. Prospect., 49, 120–127, doi:10.1046/j.1365-2478.2001.00243.x, 2001.

Bakke, N. E. and Ursin, B.: Thin-bed AVO effects, Geophys. Prospect., 46, 571–587, doi:10.1046/j.1365-2478.1998.00101.x, 1998.

Best, A. I., McCann, C., and Sothcott, J.: The relationships between the velocities, attenuations and petrophysical properties of reservoir sedimentary rocks, Geophys. Prospect., 42, 151–178, doi:10.1111/j.1365-2478.1994.tb00204.x, 1994.

Booth, A. D., Kulessa, B., Hubbard, A. L., Gusmeroli, A., Doyle, S., Dow, C. F., Jones, G., Murray, T., and Clark, R. A.: Seismic characterisation of subglacial material around a supraglacial meltwater lake, Russell Glacier, West Greenland; EGU General Assembly, Vienna, Austria, EGU2011-4682, 2011.

Bouchon, M.: A simple method to calculate Green's Functions for elastic layered media, B. Seismol. Soc. Am., 71, 959–971, 1981.

Boulton, G. S., Dobbie, K. E., and Zatsepin, S.: Sediment deformation beneath glaciers and its coupling to the subglacial hydraulic system, Quatern. Int., 86, 3–28, doi:10.1016/S1040-6182(01)00048-9, 2001.

Bradford, J. H., Nichols, J., Mikesell, T. D., and Harper, J. T.: Continuous profiles of electromagnetic wave velocity and water content in glaciers: an example from Bench Glacier, Alaska, USA, J. Glaciol., 50, 1–9, doi:http://dx.doi.org/10.3189/172756409789097540, 2009.

Clarke, G. K. C., Collins, S. G., and Thompson, D. E.: Flow, thermal structure and subglacial conditions of a surge-type glacier, Can. J. Earth Sci., 21, 232–240, 1984.

Dasgupta, R. and Clark, R. A.: Estimation of Q from surface seismic reflection data, Geophysics, 63, 2120–2128, doi:10.1190/1.1444505, 1998.





Echelmeyer, K. and Wang, Z.: Direct observation of basal sliding and deformation of basal drift at sub-freezing temperatures, J. Glaciol., 33, 83–98, 1987.

Evans, D. J. A., Phillips, E. R., Hiemstra, J. F., and Auton, C. A.: Subglacial till: Formation, sedimentary characteristics and classification, Earth-Sci. Rev., 78, 115–176, doi:10.1016/j.earscirev.2006.04.001, 2006.

Fischer, U. H. and Clark, G. K. C.: Ploughing of subglacial sediment, J. Glaciol., 40, 97–106, 1994.

Gercek, H.: Poisson's ratio values for rocks, International Journal of Rock Mechanics and Mining Sciences, 44, 1–13, doi:10.1016/j.ijrmms.2006.04.011, 2007

Gretener, P.: AVO and Poisson's ratio, The Leading Edge, 22, 70–72, 2003.

Gusmeroli, A., Clark, R. A., Murray, T., Booth, A. D., Barrett, B., and Kulessa, B.: Seismic wave attenuation in the uppermost glacier ice of Storglaciären, J. Glaciol., 54, 939–942, doi:10.3189/002214310791968485, 2010.

Hall, M.: Predicting bed thickness with cepstral decomposition, The Leading Edge, 25, 199–204, 2006.

Horgan, H. W., Anandakrishnan, S., Alley, R. B., Peters, L. E., Tsoflias, G. P., Voigt, D. E., and Winberry, J. P.: Complex fabric development revealed by englacial seismic reflectivity: Jakobshavn Isbræ, Greenland, Geophys. Res. Lett., 35, L10501, doi:10.1029/2008GL033712, 2008.

Iverson, N. R.: Shear resistance of subglacial till: hydrology rules, J. Glaciol., 56, 1104–1114, doi:10.3189/002214311796406220, 2011.

Iverson, N. R., Jansson, O., and Hooke, R. LeB.: In situ measurements of the strength of deforming subglacial till, J. Glaciol., 40, 497–503, 1994.

Iverson, N. R., Hoover, T. S., and Baker, R. W.: Ring-shear studies of till deformation: Coulomb-plastic behaviour and disturbed strain in glacier beds, J. Glaciol., 44, 634–642, 1998.

Kennet, B. L. N.: Seismic wave propagation in stratified media, Cambridge University Press, 1983.

Kennet, B. L. N. and Kerry, H. J.: Seismic waves in a stratified half-space, Geophys. J. Roy. Astr. Soc., 57, 557–583, 1979.

King, E. C., Smith, A. M., Murray, T., and Stuart, G. W.: Glacier-bed characteristics of midtre Lovénbreen, Svalbard, from high-resolution seismic and radar surveying, J. Glaciol., 54, 145–156, doi:10.3189/002214308784409099, 2003.

Kohnen, H.: The temperature dependence of seismic waves in ice, J. Glaciol., 13, 144–147,

1974.
Kulessa, B., Stuart, G., Hobbs, A., and Booth, A. D.: Subglacial hydromechanical processes from seismic amplitude verses offset (AVO) monitoring, European Geosciences Union General Assembly, Vienna, Austria, EGU2008-A-06080, 2008.
Lin, L. and Phair, R.: AVO tuning, 63rd Society of Exploration Geophysicists Meeting, Washington DC, USA, Expanded Abstracts, 727–730, 1993.
Lindsey, J. P.: The Fresnel zone and its interpretive significance, The Leading Edge, 8, 33–39, 1989.
Mallick, S. and Frazer, N. L.: Practical aspects of reflectivity modelling, Geophysics, 52, 1355–1364, doi:10.1190/1.1442248, 1987.
Morozov, I. B.: Anelastic acoustic impedance and the correspondence principle, Geophys. Prospect., 59, 24–34, doi:10.1111/j.1365-2478.2010.00890.x, 2011.
Nolan, M. and Echelmeyer, K.: Seismic detection of transient changes beneath Black Rapids Glacier, Alaska, USA: II. Basal Morphology and processes, J. Glaciol., 45, 132–146, 1999.
Odebeatu, E., Zhang, J., Chapman, M., and Li, X.-Y.: Application of spectral decomposition to detection of dispersion anomalies associated with gas saturation, The Leading Edge, 25, 206–210, 2006.
Pattyn, F.: Numerical modelling of a fast-flowing outlet glacier: experiments with different basal conditions, Ann. Glaciol., 23, 237–246, 1996.
Perroud, H. and Tygel, M.: Nonstretch NMO, Geophysics, 69, 599–607, doi:10.1190/1.1707080, 2004.
Peters, L. E. and Anandakrishnan, S.: Measurements of seismic attenuation in ice: A potential proxy for englacial temperature?, American Geophysical Union, Fall Meeting 2010, San Francisco, USA, C21A-0511, 2010.
Peters, L. E., Anandakrishnan, S., Alley, R. B., and Smith, A. M.: Extensive storage of basal meltwater in the onset region of a major West Antarctic ice stream, Geology, 35, 251–254, doi:10.1130/G23222A.1, 2007.
Peters, L. E., Anandakrishnan, S., Holland, C. W., Horgan, H. J., Blakenship, D. D., and Voigt, D. D.: Seismic detection of a subglacial lake near South Pole, Antarctica, Geophys. Res. Lett., 35, L23501, doi:10.1029/2008GL035704, 2008.
Piotrowski, J. A., Larsen, N. K., and Junge, F. W.: Reflections on soft subglacial beds as a mosaic of deforming and stable spots, Quaternary Sci. Rev., 23, 993–1000, doi:10.1016/j.quascirev.2004.01.006, 2004.



Pimentel, S., Flowers, G. E., and Schoof, G. E.: A hydrologically coupled higher-order flow-band model of ice dynamics with a Coulomb friction sliding law, J. Geophys. Res., 115, F04023, doi:10.1029/2009JF001621, 2010.
Porter, P. R. and Murray, T.; Mechanical and hydraulic properties of till beneath Bakaninbreen, Svalbard, J. Glaciol., 47, 167–175, doi:10.3189/172756501781832304, 2001.
Quintal, B., Schmalholz, S. M., and Podladchikov, Y. Y.: Low-frequency reflections from a thin layer with high attenuation caused by interlayer flow, Geophysics, 74, N15–N23, doi:10.1190/1.3026620, 2009.
Reinardy, B. T. I., Larter, R. D., Hillenbrand, C.-D., Murray, T., Hiemstra, J. F., and Booth, A.: Steaming flow of an Antarctic Peninsula palaeo ice-stream by both basal sliding and deformation of substrate, J. Glaciol., 57, 596–608, doi:10.3189/002214311797409758, 2011.
Richards, M. A.: Seismic evidence for a weak basal layer during the 1982 surge of Variegated Glacier, Alaska, USA, J. Glaciol., 34, 111–120, 1982.
Riedel, M. and Theilen, F.: AVO investigations of shallow marine sediments, Geophys. Prospect., 49, 198–212, doi:10.1046/j.1365-2478.2001.00246.x, 2001.
Rubino, J. G. and Velis, D.: Thin-bed prestack spectral inversion, Geophysics, 74, R49–R57, doi:10.1190/1.3148002, 2009.
Sain, K. and Singh, A. K.: Seismic quality factors across a bottom simulating reflector in the Makran Accretionary Prism, Arabian Sea, Mar. Pet. Geol., 28, 1838–1843, doi:10.1016/j.marpetgeo.2011.03.013, 2011.
Sarkar, D. S. and Tsvankin, I.: Migration velocity analysis in factorized VTI media, Geophysics, 69, 708–718, doi:10.1190/1.1759457, 2004.
Sergienko, O. and Hulbe, C. L.: "Sticky spots" and subglacial lakes under ice streams of the Siple Coast, Antarctica, Ann. Glaciol., 52, 18–22, 2011.
Sheriff, R. E. and Geldart, L. P.: Exploration Seismology; Cambridge University Press, 2nd Edition, 1999.
Shuey, R. T.: A simplification of the Zoeppritz equations, Geophysics, 50, 609–614, doi:10.1190/1.1441936, 1985.
Simm, R., White, R., and Uden, R.: The anatomy of AVO crossplots; The Leading Edge, February, 150–155, doi:10.1190/1.1438557, 2000.
Smith, A. M.: Basal conditions on Rutford Ice Stream, West Antarctica, from seismic observations, J. Geophys. Res., 102, 435–552, doi:10.1029/96JB02933, 1997.
Smith, A. M.: Subglacial bed properties from normal-incidence seismic reflection data, J. Env.

Eng. Geoph., 12, 3–13, doi:10.2113/JEEG12.1.3, 2007.
Swan, H. W.: Amplitude-versus-offset measurement errors in a finely layered medium, Geophysics, 64, 678–690, doi:10.1190/1.1442956, 1991.
Truffer, M., Echelmeyer, K., and Harrison, W. D.: Implications of till deformation on glacier dynamics; J. Glaciol., 47, 123–134, doi:10.3189/172756501781832449, 2001.
Tsvankin, I.: Seismic Signatures and Analysis of Reflection Data in Anisotropic Media; Handbook of Geophysical Exploration, Seismic Exploration, edited by: Helbig, K. and Treitel, S., Pergamon, The Netherlands, 2001.
Vaughan, D. G., Smith, A. M., Nath, P. N., and Le Meur, E.; Acoustic impedance and basal shear stress beneath four Antarctic ice streams, Ann. Glaciol., 36, 225–232, doi:10.3189/172756403781816437, 2003.
Widess, M. B.: How thin is a thin bed?, Geophysics, 38, 1176–1180, doi:10.1190/1.1440403, 2003.



**Table 1.** Model properties for example AVA curves in Fig. 1. In Fig. 1a, Poisson's ratio ($\nu$) is fixed at 0.4; in Fig. 1b, acoustic impedance ($Z$) is fixed at $3.3 \times 10^6\,\mathrm{kg\,m^{-2}\,s^{-1}}$. Acoustic impedance for ice, bedrock and water are $3.5 \times 10^6\,\mathrm{kg\,m^{-2}\,s^{-1}}$, $14.0 \times 10^6\,\mathrm{kg\,m^{-2}\,s^{-1}}$ and $1.5 \times 10^6\,\mathrm{kg\,m^{-2}\,s^{-1}}$ respectively; corresponding Poisson's ratios are 0.333, 0.296 and 0.500 (e.g. Peters et al., 2008).

| Model | Fig. 1a; $\nu$ fixed at 0.4 | Fig. 1b; $Z$ fixed at $3.3 \times 10^6\,\mathrm{kg\,m^{-2}\,s^{-1}}$ |
|---|---|---|
| | $Z$ (x $10^6\,\mathrm{kg\,m^{-2}\,s^{-1}}$) | $\nu$ (dimensionless) |
| *i* | 3.0 | 0.1 |
| *ii* | 3.5 | 0.2 |
| *iii* | 4.0 | 0.3 |
| *iv* | 4.5 | 0.4 |
| *v* | 5.0 | 0.5 (water; theoretical maximum) |

**Table 2.** Ice and till properties as used in *SKB2* forward-modelling of seismic data. Ice properties are fixed throughout, and three pairs of quality factors ($Q_\infty$, $Q_H$ and $Q_L$) are assumed for the subglacial till. Eight thicknesses of dilatant till are simulated, giving a total of 24 synthetic seismic responses.

| Quantity | | ICE | DILATANT TILL | LODGED TILL |
|---|---|---|---|---|
| thickness (m) | | 1000 | 0.1, 0.3, 0.5, 1.0, 1.5, 2.0, 2.5, 3.0 | *halfspace* |
| $v_P$ ($m\,s^{-1}$) | | 3800 | 1800 | 1950 |
| $v_S$ ($m\,s^{-1}$) | | 1900 | 200 | 1000 |
| density ($kg\,m^{-3}$) | | 920 | 1900 | 2000 |
| acoustic impedance (x $10^6$ $kg\,m^{-2}\,s^{-1}$) | | 3.50 | 3.42 | 3.90 |
| Poisson's ratio | | 0.333 | 0.494 | 0.322 |
| P-wave quality factor | $Q_\infty$ | 430 | $10^4$ | $10^4$ |
| | $Q_H$ | | 115 | 115 |
| | $Q_L$ | | 15 | 15 |
| S-wave quality factor | $Q_\infty$ | 430 | $10^4$ | $10^4$ |
| | $Q_H$ | | 42 | 42 |
| | $Q_L$ | | 8 | 8 |



**Table 3.** Apparent acoustic impedance, $Z_{app}$, and Poisson's ratio, $\sigma_{app}$, as measured from Fig. 5 if reflectivity was allocated to a single till layer. *dZ* and *dσ* show the error between observed and model properties.

| | $Q_\infty$ | | | $Q_H$ | | | $Q_L$ | | |
|---|---|---|---|---|---|---|---|---|---|
| $h_d(m)$ | $Z_{app} \times 10^6$ $kg\,m^{-2}\,s^1$ | *dZ* (%) *(dilatant)* | *dZ* (%) *(lodged)* | $Z_{app} \times 10^6$ $kg\,m^{-2}\,s^1$ | *dZ* (%) *(dilatant)* | *dZ* (%) *(lodged)* | $Z_{app} \times 10^6$ $kg\,m^{-2}\,s^1$ | *dZ* (%) *(dilatant)* | *dZ* (%) *(lodged)* |
| 0.1 | 3.90 | +14.0 | +0.0 | 3.82 | +11.7 | −2.1 | 3.17 | −7.3 | −18.7 |
| 0.3 | 3.89 | +13.7 | −0.3 | 3.81 | +11.4 | −2.3 | 3.26 | −4.7 | −16.4 |
| 0.5 | 3.91 | +14.3 | +0.3 | 3.83 | +12.0 | −1.8 | 3.23 | −5.6 | −17.2 |
| 1.0 | 4.02 | +17.5 | +3.1 | 4.04 | +18.1 | +3.6 | 3.09 | −9.6 | −20.8 |
| 1.5 | 4.18 | +22.2 | +7.2 | 4.37 | +27.8 | +12.1 | 3.03 | −11.4 | −22.3 |
| 2.0 | 4.35 | +27.2 | +11.5 | 4.65 | +36.0 | +19.2 | 2.97 | −13.2 | −23.8 |
| 2.5 | 3.47 | +1.5 | −11.0 | 3.42 | +0.0 | −12.3 | 2.94 | −14.0 | −24.6 |
| 3.0 | 3.46 | +1.2 | −11.3 | 3.40 | −0.6 | −12.8 | 2.91 | −14.9 | −25.4 |
| | $\sigma_{app}$ | *dσ* (%) *(dilatant)* | *dσ* (%) *(lodged)* | $\sigma_{app}$ | *dσ* (%) *(dilatant)* | *dσ* (%) *(lodged)* | $\sigma_{app}$ | *dσ* (%) *(dilatant)* | *dσ* (%) *(lodged)* |
| 0.1 | 0.424 | −14.2 | +31.6 | 0.422 | −14.6 | +31.1 | 0.464 | −6.1 | +44.1 |
| 0.3 | 0.442 | −10.5 | +37.3 | 0.455 | −7.9 | +41.3 | 0.474 | −4.0 | +47.2 |
| 0.5 | 0.456 | −7.7 | +41.6 | 0.456 | −7.7 | +41.6 | 0.474 | −4.0 | +47.2 |
| 1.0 | 0.456 | −7.7 | +41.6 | 0.461 | −6.7 | +43.2 | 0.482 | −2.4 | +49.7 |
| 1.5 | 0.458 | −7.3 | +42.2 | 0.460 | −6.9 | +42.9 | 0.478 | −3.2 | +48.4 |
| 2.0 | 0.462 | −6.5 | +43.5 | 0.458 | −7.3 | +42.2 | 0.473 | −4.3 | +46.9 |
| 2.5 | 0.470 | −4.9 | +46.0 | 0.485 | −1.8 | +50.6 | 0.482 | −2.4 | +49.7 |
| 3.0 | 0.470 | −4.9 | +46.0 | 0.485 | −1.8 | +50.6 | 0.477 | −3.4 | +48.1 |

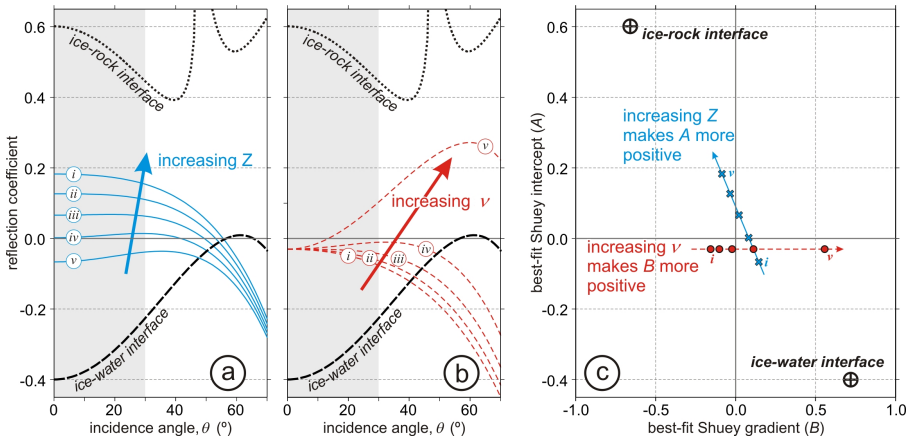


**Fig. 1.** Example amplitude versus angle (AVA) responses for glacier beds overlying till units with acoustic impedance and Poissons ratio as specific in Table 1. **(a)** Acoustic impedance is varied, while Poissons ratio is fixed. **(b)** Poissons ratio is varied while acoustic impedance is fixed. Black curves denote example cases of ice-water and ice-rock interfaces (the latter undergoing critical refraction at ~47°). **(c)** AVA cross-plot of best-fit Shuey terms. Blue crosses plot data from **(a)**, red circles plot data from **(b)**. Black curves and symbols show reference models of ice-water and ice-bedrock interfaces. Best-fit terms are calculated only for the first 30° of incidence (grey shading in **a** and **b**).





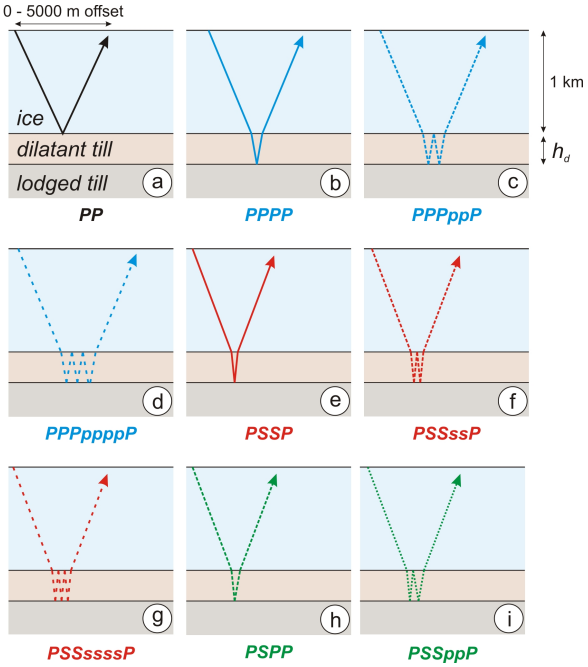


**Fig. 2.** Nomenclature and schematic representation of raypaths considered in modelling. Line colours and styles are equivalent to those in successive figures. Raypath **(a)** is the basal ice reflection (black), **(b–d)** comprise P-wave propagation along the whole travel-path (blue), **(e–g)** have S-wave mode conversions within the dilatant till (red), and **(h)** and **(i)** convert between S- and P-wave modes within the dilatant till (green).

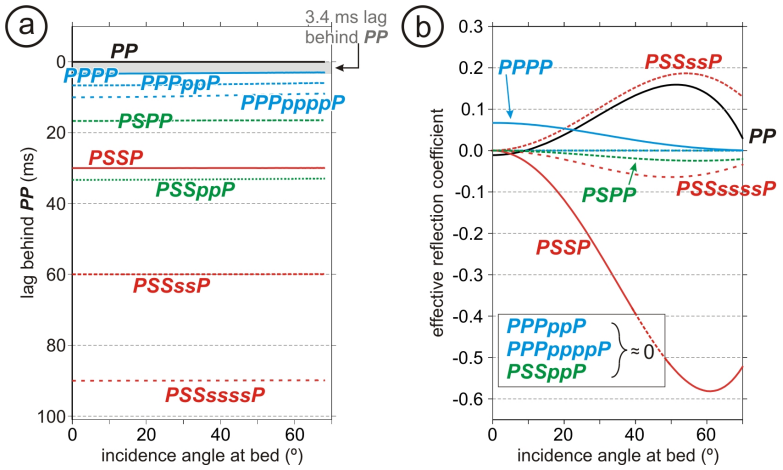


**Fig. 3.** Travel-time and effective reflectivity for model raypaths, as introduced in Fig. 2. **(a)** Ray-traced travel-times expressed, for clarity, as a lag behind ***PP***. Raypaths that arrive after a lag of 3.4 ms (grey shading) cannot contribute to the composite reflectivity. **(b)** Effective reflectivity of reflections in **(a)**. Raypaths that feature intrabed P-wave multiples have negligible reflectivity.





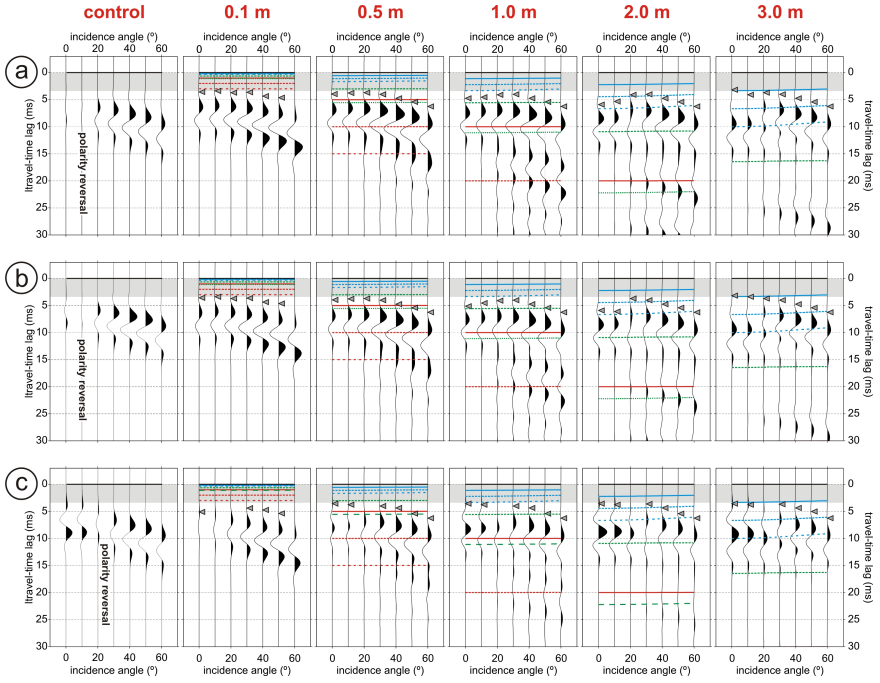


**Fig. 4.** Synthetic seismic responses to thin layers of varying $h_d$ (from 0.1 to 3.0 m) for **(a)** $Q_\infty$ **(b)** $Q_H$ and **(c)** $Q_L$ attenuation models. Traces are non-stretch NMO corrected, and amplitudes are corrected for attenuation losses and geometric spreading; ray-traced travel-time models are included, and the grey-shading shows the threshold of interference. Control responses show reflections from ice overlying a dilatant till half-space. Grey triangles show the location of amplitude picks used to generate AVA curves in Fig. 5.

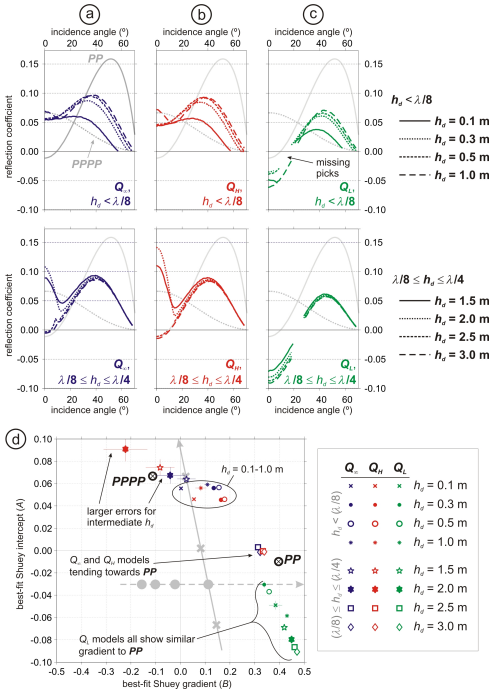


**Fig. 5.** AVA responses for $Q_\infty$, $Q_H$ and $Q_L$ seismic (**a**, **b** and **c**, respectively; upper row shows $h_d < \lambda/8$, lower row shows $\lambda/8 \leq h_d \leq \lambda/4$). Grey curves show effective reflectivities for ***PP*** and ***PPPP***, for reference. Picking is ambiguous in $Q_L$ responses close to polarity reversals hence picks are omitted. **(d)** AVA cross-plot for reflectivities in **(a–c)**. For reference, the example models from Fig. 1c are also plotted (light grey).



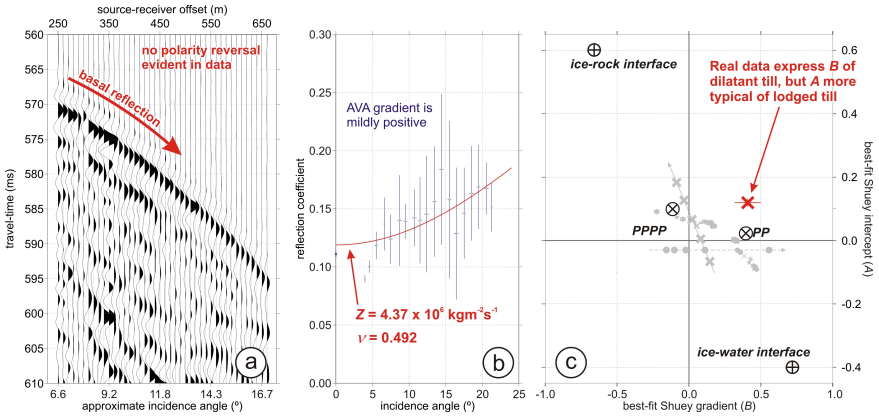


**Fig. 6.** AVA analysis of real data. from Russell Glacier, Greenland. **(a)** Representative seismic record; the basal reflection exhibits no polarity reversal across the offset range. **(b)** AVA response of the basal reflection. Implied acoustic impedance is suggestive of lodged till, whereas Poissons ratio suggests dilatant till. **(c)** AVA cross-plot showing the characteristics of real data (red) compared to reference reflectivties (black) and model responses in Fig. 5 (light grey). Note that the error in *A* is negligible.